

Biostimulation of Biogenic Zinc Oxide Nanoparticles on Morpho-Physiological Development of Basil Seedlings

Semra Kilic^{1*}, Sercan Önder², Damla Önder¹, Havva Kaya³

¹ Suleyman Demirel University, Department of Biology, Isparta, TÜRKİYE

<https://orcid.org/0000-0001-9494-2952>

*corresponding author: semrakilic@sdu.edu.tr

² Isparta University of Applied Sciences, Department of Agricultural Biotechnology, Isparta,

TÜRKİYE

<https://orcid.org/0000-0002-8065-288X>

³ Suleyman Demirel University, Department of Bioengineering, Isparta, TÜRKİYE

<https://orcid.org/0000-0001-7083-0542>

(Received: 10.12.2024, Accepted: 19.02.2025, Published: 25.05.2025)

Abstract: Nanomaterials derived from essential nutrients such as zinc enable the synthesis of nanocomposite materials and nano-fertilizers, offering broader agricultural applications and improved human nutrition. In this study, thyme leaf extract was used to synthesize biogenic zinc-oxide nanoparticles (BZO-NPs), and their effects on the micro-morphological and biochemical parameters of sweet basil (*Ocimum basilicum* L.) were investigated. The synthesized BZO-NPs were characterized using UV-Vis spectroscopy, scanning electron microscopy (SEM), X-ray powder diffraction (XRD), and energy-dispersive X-ray spectroscopy (EDXS). The BZO-NPs exhibited a crystalline spherical structure with sizes ranging from 50 to 100 nm. Different BZO-NP concentrations (25, 50, 100, and 200 mg L⁻¹) were applied to basil plants during the vegetative growth stage. The relative growth rate, total chlorophyll content, and relative water content ratio increased at all BZO-NP concentrations except 200 mg L⁻¹, with the highest values observed at 50 mg L⁻¹ BZO-NP. Stomata density decreased at all BZO-NP concentrations except 50 mg L⁻¹ BZO-NP, and stomata sizes also decreased at all BZO-NP concentrations. The number of peltate trichomes increased on both leaf surfaces with higher BZO-NP concentrations, with a more pronounced increase on the upper leaf surface. Changes in peltate trichomes were associated with the presence of three phenolic compounds: caffeic acid, rosmarinic acid, and chlorogenic acid. The treatment of BZO-NP concentrations also influenced the activity of antioxidant enzymes (SOD, CAT, GR and APX) in sweet basil. Treatment with BZO-NPs at all concentrations reduced oxidative stress by decreasing hydrogen peroxide levels compared to the control, while malondialdehyde (MDA) content remained unchanged. In conclusion, BZO-NPs, being economically viable and environmentally sustainable, demonstrate significant potential as nano-based nutrient sources for basil cultivation.

Key words: Antioxidant enzymes, Basil, Glandular trichomes, Phytochemicals, Stomata

1. Introduction

Zinc is a microelement that regulates various metabolic activities and cellular functions in plants, serving as an essential component of numerous proteins. As a key constituent of over 300 enzymes involved in protein synthesis and growth regulation [1], zinc deficiency can lead to various physiological symptoms in plants. These symptoms include growth disorders in root and stem, leaf necrosis or chlorosis, and impaired photosynthesis [2]. Zn deficiency is particularly prevalent in alkaline soils, where arid and semi-arid climates reduce the availability of zinc over time [3]. In recent years, nanotechnology has emerged as a widely accepted, effective, and multifunctional approach in biological sciences, including agriculture [4]. In agriculture applications, nanoparticles (NPs) are being explored as nanofertilizers, nanopesticides, and delivery systems for plant growth regulators due to their large surface area to volume ratio, nanoscale size, structural versatility, and ability to effectively transport chemicals into cells [5]. Among these, metal oxide NPs have garnered significant attention from agricultural scientists due to their high performance, cost-effectiveness, and sustainability [6]. However, excessive or uncontrolled use of NPs can induce oxidative stress in plant, potentially leading to harmful effects [7]. Therefore, further research is necessary to identify suitable NPs, understand their mechanisms of action in plants, optimize particle size, and determine effective and cost-efficient dosages tailored to specific plant species [8]. Recent studies have highlighted the potential of Zinc Oxide Nanoparticles (ZnO-NP's) as promoters of growth and development, mitigators of abiotic stress, and inducers of morphological and physiological changes [9, 10]. Despite these advancements, the effect of biogenic zinc oxide nanoparticles (BZO-NPs) on the micro-morphological structure and biochemical processes in basil seedlings remain unexplored. In this study, the optimal Zn concentration and plant-enhancer effects were investigated by applying different concentrations of BZO-NPs to basil seedlings. The study focused on characterizing BZO-NPs and examining their micro-morphological and biochemical impacts on basil seedlings.

2. Material and Method

2.1. Preparation of plant materials and extracts

BZO-NPs used for the experiments were synthesized using thyme leaves (*Origanum minutiflorum* O. Schwarz & P. H. Davis). *O. minutiflorum* leaves were provided in July from the Sütçüler district of Isparta. The samples were cleaned of any residue and dust by washing them twice with sterile water before drying for two days at room temperature

in the shade. The dried samples were ground using a coffee grinder, and the sample (1 g) was incubated in water at 100 °C for 20 min. The aliquot was then extracted with Whatman (No. 1). The extracts were cooled to room temperature for use as reducing agents to Zn²⁺.

2.2. Biosynthesis of BZO-NPs

Phytonanosynthesis of ZnO-NPs was prepared by stirring 0.1 M zinc chloride (ZnCl₂.4H₂O) in 100 mL of ddH₂O at 600 rpm. Thyme extract (50 mL) was added to 50 mL of ZnCl₂ and stirred at 200 rpm for 24 h at 25 °C and then a white precipitate was obtained. The mixture was centrifuged at 600 rpm for 15 min and the resulting white pellet was washed three times with ddH₂O and centrifuged. The ultimate white pellet was dried under vacuum and stored at +4 °C until the characterization tests of NPs and treatment to basil seedlings.

2.3. Morphological characterizations of BZO-NPs

The following techniques were used to characterize the synthesized NPs: UV-Vis spectroscopy (200-800 nm range) was employed to confirm the formation and optical properties of BZO-NPs. The presence and crystal structure of the synthesized BZO-NPs were determined using X-ray powder diffraction (XRD) with a X'Pert-PRO advanced diffractometer, utilizing Cu K α ($\lambda = 1.5406 \text{ \AA}$) radiation, 40 kV, 30 mA and 2θ scanning range of 10°-90°. The crystal structure was confirmed by observing sharp Bragg reflection in the XRD patterns. Crystal structure determination was further supported by the Joint Committee on Powder Diffraction Standards (JCPDS) library. The size and morphology of the synthesized BZO-NPs were examined using scanning electron microscopy (SEM), while energy-dispersive-X-ray spectroscopy (EDS) was used to determine the elemental composition and purity of the NPs.

2.4. Treatment of BZO-NPs to basil seedlings

Basil seeds were grown into seedlings for 20 days in plastic pots containing a mixture of sand, forest-soil, and organic substrate (1:1:1). BZO-NPs at different concentrations (25, 50, 100 and 200 mg L⁻¹) were applied once to the basil seedlings as a 100 mL solution, and the seedlings were watered weekly for 6 months. In the control group, only water was used. The seedlings were grown in a plant growth chamber with a light intensity of 160 $\mu\text{mol/m}^{-2}/\text{s}^{-1}$, 70-80% relative humidity, and a temperature regime of 28 °C during the

day and 22 °C at night. Morpho-physiological changes induced by BZO-NP treatment in basil seedlings were identified.

2.5. Micro-morphological parameters

The seedlings were dried for 48 h at 105 ° C after their fresh weights were specified using precision scale. The relative growth rates (RGR) of the seedlings were calculated according to the formula below [11];

$$\text{RGR}(\%) = \left[\frac{\text{Dry Weight}}{\text{Fresh Weight}} \right] \times 100 \quad (1)$$

Thirty leaf samples were transferred onto graph paper and weighed (x) from seedlings in each treatment group. The same graph paper was also used to cut 1 cm², which was then weighed (y). The leaf area (LA) was calculated using the equation below and expressed as m² kg⁻¹ [12];

$$\text{LA} = \frac{x}{y} \quad (2)$$

Fresh leaf sample (approximately 3 g, FW) was submerged in pure water for a full day, and once a piece of towel paper had absorbed the surplus water on the leaf surface, the turgor weight (TW) was measured. The samples from which turgor weight was taken were incubated at 65 °C for 24 h and then their dry weight (DW) was weighed. The relative water content (RWC) was calculated according to the formula below [13];

$$\text{RWC}(\%) = \left[\frac{\text{FW}-\text{DW}}{\text{TW}-\text{DW}} \right] \times 100 \quad (3)$$

The stomata index (SI) on the leaves was performed according to Rengifo et al. (2002) [14]. The number of stomata (S) and epidermal cells (E) on 1 mm² areas (approximately 50 areas) of the adaxial and abaxial surfaces of the leaves were counted under light microscope and computed using the formula below;

$$\text{SI}(\%) = \left[\frac{S}{E + S} \right] \times 100 \quad (4)$$

Stomatal width (Wg) and stomatal length (Lg) on 1 mm² areas (approximately 50 areas) of leaf surfaces were measured under a light microscope and the stomatal area (SA) was calculated according to the formula below [15];

$$\text{SA} (\mu\text{m}^2) = \left[\pi \times \frac{\text{Wg} \times \text{Lg}}{4} \right] \quad (5)$$

To evaluate the stomatal density (SD, the number of stomata in an area) of leaves, superficial sections of 1 mm² were obtained from the leaf's upper and lower surfaces, and at least three leaves were examined using a light microscope to obtain the mean SD value. The relative ratio of the total stomatal pore area to the leaf area is known as the stomatal pore index (SPI). The SPI ratio was computed using the following formula after determining the stomatal density (SD) and length (Lg) on both leaf surfaces [16].

$$\text{SPI} = \text{Stomata Density (SD)} \times (\text{Stomata Length (Lg)})^2 \quad (6)$$

The morphology and distribution of peltate and capitate trichomes (gland trichomes) on both surfaces of basil leaves were measured according to Turner et al. (2000) [17]. Submicroscopic structures of trichomes and stomata on the adaxial and abaxial surfaces of the leaves were examined using SEM (LEO Stereoscan 360).

2.6. Biochemical parameters

Essential oil components were determined using HS-SPME-GC-MS. Dry basil leaves (1 g) were ground into powder, and extraction was performed via solid-phase microextraction (SPME) using a 75 µm-thick layer fiber precoated with divinylbenzene/carboxen/polydimethylsiloxane. Prior to extraction, the SPME fibers were reconditioned for thermal desorption at 260 °C for 5 min, and each sample was manually inserted into the septum and exposed to 250 °C for 5 min. Essential oil extraction was performed by incubating the samples at 80 °C for 5 min, followed by 10 min of magnetic stirring. The SPME fiber was then removed from the vial and injected for 3 min into a gas chromatography-mass spectrometry (GC-MS) analysis. Analyses were conducted using a PerkinElmer GC-MS (Norwalk, USA) instrument equipped with a BP-5 silica capillary column (30 m × 0.32 mm × 0.25 µm). The detector and injector temperature were set to 260 °C, the initial column temperature was held at 35 °C for 3 min, then gradually increased to 140 °C at 5 °C min⁻¹, and finally held at 250 °C for 10 min. The carrier gas was helium with a flow rate of 1.4 mL min⁻¹ and a split ratio of 1:50. Constituents were identified using mass spectra and linear retention indices from the Wiley, NIST Tutor, Flavors and Fragrances of Natural and Synthetic Compounds 3.0 libraries. Quantitative determination was performed using a Gas Chromatography/Flame Ionization Detector (GC-FID) under identical conditions to GC-MS. The amount of essential oil components was determined as the average of three replicates.

The leaf sample (1 g) was homogenized in 10 mL of methanol and centrifuged at 4000 rpm for 5 min. Methanol in the supernatant was removed using a rotary vacuum evaporator at 40 °C. The resulting residue was dissolved in 500 µL of methanol and then filtered through a 0.02 µm Millipore filter. The phenolic components of the extracts were evaluated using reversed-phase high-performance liquid chromatography (RP-HPLC). The Agilent 1200 HPLC system consisted of a UV detector, SIL-10A Dvp-auto-sampler, LC-10A Dvp-pump, and CTO-10 Avp column heater (Shimadzu, Kyoto, Japan). The chromatographic separation was performed with an Agilent Eclipse XDB-C18 column (250 mm × 4.60 mm × 5 µm), and the eluates were monitored at 278 nm. The mobile phase consisted of solvent A (3% acetic acid) and solvent B (80% methanol). The phenolic compounds were isolated using a modified gradient elution at 30 °C with a flow rate of 0.8 mL min⁻¹ and an injection volume of 20 µL, and the mobile phase composition was reset to the initial value after 55 min. The amount of phenolic compounds in the samples was determined based on comparisons with pure standards and retention times.

Chlorophyll content in approximately fifty basil leaves in each treatment group was measured using SPAD-502 (Minolta Co. Ltd., Japan).

Liquid nitrogen was used to pulverize 1 g of basil leaves and homogenized in 10 mL of 0.1% trichloroacetic acid (TCA). H₂O₂ and MDA contents were measured from the supernatant after the homogenate was centrifuged at 13,000 rpm for 20 min at 4 °C. The H₂O₂ content in the extracts was measured according to Velikova et al. (2000) [18]. 0.5 mL of 0.1 M potassium phosphate buffer (pH 7.0) and 2 mL of 1 M potassium iodide were added to 0.5 mL of supernatant and incubated in the dark for 1 h. The absorbance values were obtained at 390 nm using ddH₂O as a blank. H₂O₂ content was expressed as micromole H₂O₂ equivalent per gram.

A lipid peroxidation indicator called malondialdehyde (MDA) analysis was measured following Heath and Packer (1968) [19]. The solution of 4.5 mL containing 0.5% 2-thiobarbituric acid (TBA) in 20% TCA was mixed with 1 mL of extract, and the mixture was transferred to an ice bath immediately after boiling for 30 min. The reaction was centrifuged at 10,000 rpm for 10 min and absorbance was measured at 532 nm and 600 nm. The extinction coefficient used to compute the amount of MDA was 155 mM cm⁻¹.

2.6.1. Antioxidant enzyme activities

Two grams of basil leaves were pulverized in liquid nitrogen and homogenized with 0.2 grams of PVPP in 10 mL ice-cold sodium phosphate (50 mM, pH 6.4, extraction buffer) to extract superoxide dismutase (SOD), catalase (CAT), glutathione reductase (GR), and ascorbate peroxidase (APX). APX extraction was performed by adding 1 mM ascorbic acid to the extraction buffer. The resulting homogenates were centrifuged at 4 °C 15.000 rpm for 20 min. The aliquots were reserved at -20 °C in the dark until they were analyzed.

SOD was measured by inhibition of photoreduction of nitro-tetrazolium following Giannopolitis and Ries (1977) [20]. The components of the reaction mixture were 2.8 mL of reaction solvent (0.1 mM EDTA, 13 mM methionine, 50 mM sodium carbonate, 75 μ M nitroblue-tetrazolium, 50 mM sodium phosphate (pH 7.8)), 0.1 mL of 2 mM riboflavin, and 0.1 mL of supernatant. The reaction was incubated under 15 W white-fluorescent lamps for 15 min, and the control prepared with ddH₂O was incubated in the dark. One unit of SOD activity was calculated by measuring the 50% inhibition absorbance of nitroblue-tetrazolium reduction at 560 nm.

CAT was measured following Chance and Maehly (1955) [21]. The reaction components were 0.1 mL supernatant, 2.9 mL of 50 mM sodium phosphate (pH 7.0), and 40 mM H₂O₂. The decrease in absorbance was determined at 240 nm ($\epsilon_{240} = 36 \text{ M}^{-1} \text{ cm}^{-1}$) for 3 min. One unit was measured by H₂O₂ decomposition per min.

GR was determined according to Chance and Maehly (1955) [21]. The reaction included 0.1 mL of supernatant, 500 μ L of 2 mM oxidized glutathione, and 350 μ L of 0.1 M sodium phosphate (pH 7.8). The reaction was initiated by adding 50 μ L of 2.4 mM NADPH and the absorbance of the decreasing NADPH was measured at 340 nm ($\epsilon_{340} = 6.22 \text{ mM}^{-1} \text{ cm}^{-1}$) for 3 min. One unit was measured as an oxidation of 1 mmol NADPH per min.

APX was performed using the procedure described by Nakano and Asada (1981) [22]. The reaction was initiated by inserting 700 μ L of reaction buffer (0.1 mM EDTA Na₂, 0.5 mM ascorbate, 50 mM sodium phosphate (pH 7.0)) and 200 μ L of 1.2 mM H₂O₂ to the 0.1 mL of enzyme extract. The decrease in absorbance was determined at 290 nm ($\epsilon_{290} = 2.8 \text{ mM}^{-1} \text{ cm}^{-1}$) for 3 min. One unit was measured at 1 mmol H₂O₂ decomposition per min.

The Bradford method [23] was used to calculate the protein concentration of antioxidant enzyme extracts, and the activity of each antioxidant enzyme was measured in U mg protein⁻¹.

2.7. Statistical analysis

Minitab software (Minitab version 19, Philadelphia, USA) was used to perform analysis of variance (ANOVA) on micro-morphological and biochemical data. Tukey's ($p \leq 0.05$) was employed to discriminate differences between means. All values were denoted as mean \pm standard deviation. OriginPro software (OriginLab, Northampton) was used to calculate the Pearson linear correlation.

3. Results and Discussion

Phytochemicals such as phenolic compounds, flavonoids, amides, alkenes, and proteins in the aqueous extract prepared with thyme leaves are responsible for the biosynthesis of BZO-NP due to their ability to stabilize metal nanostructures, capping and adjusting their morphology and size. In this study, BZO was synthesized for the first time using these endemic thyme leaf extracts, and its characterization was made using the following analytical methods.

Morphological Characterization of BZO-NPs

Structural and morphological properties of green-synthesized BZO-NPs were examined using UV-Vis spectroscopy, XRD and SEM. The formation of a white precipitate in the mixture, prepared using thyme leaf extract and zinc chloride ($\text{ZnCl}_2 \cdot 4\text{H}_2\text{O}$) solution, indicated the presence of BZO-NPs through the reduction of Zn^{2+} ions (Figure 1a). The color change from light yellow to white, which signifies the reduction of zinc ions in the extract, resulting from the excitation of free electrons in phenolic compounds by metallic nanoparticles [24]. Polyphenols, which act as both reducing and stabilizing agents in the plant extract, react with the zinc ions in the solution, reducing them to their zero-valent state. The maximum optical absorption band observed at 360 nm corresponds to the exposure, excitation, and absorption of zinc colloid nanoparticles, confirming that thyme leaf extract facilitates the reduction of zinc ions. Additionally, the detection of a peak in the wavelength range at ~ 370 nm clearly indicates the presence of BZO-NPs in the reaction mixture. This peak arises from the excitation of electrons from a filled orbital to

an empty anti-bonding orbital, driven by energy associated with the specific wavelength of light [25].

The crystal structure of the BZO-NPs made using thyme extract was ascertained through X-ray diffraction investigations conducted. In the XRD model, the peaks of Bragg reflections are defined by the number of (1 1 1), (2 0 0), (2 2 0), (3 1 1), (2 2 2), (4 0 0) reflections corresponding to 33.5° , 38.87° , 56.15° , 66.99° , 70.4° and 83.46° at 2θ , respectively (Figure 1b). These observed peaks proved the synthesized BZO-NPs' crystal structure. Various Bragg reflections prove that the thyme extract used as a reducing agent stabilizes the produced nanoparticles, confirming the crystallization bioorganic phase occurring on the surface of BZO-NPs [26]. These obtained planes are compatible with the spherical structure corresponding to pure BZO-NPs according to the JCPDS (ICSD#897102) file.

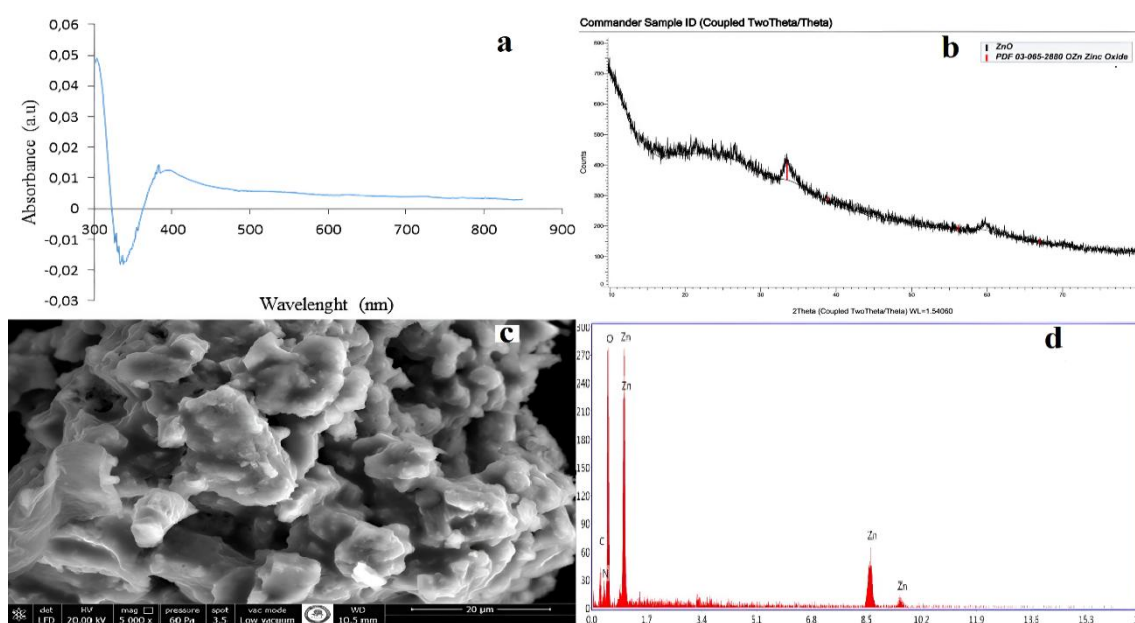


Figure 1. Characterization tests of BZO-NPs; a) UV-Vis absorption spectra, b) XRD, c) SEM image and d) EDS spectra

Although the majority of the biosynthesized BZO-NPs were spherical nanoparticles between 50 and 100 nm in size, irregular morphology nanoparticles were also found; these aggregated into larger particles between 130 and 150 nm as a result of smaller particles joining to form large particles (Figure 1c). The resulting nanoparticles appear larger than their actual size because the hydrodynamic layers that form around the particle in the liquid medium lead to the formation of large-sized and nanoaggregates [27]. Moreover, organic molecules in the leaf extract which stuck in clustered form due to the presence of irregular nanoparticles, the polarity of nanoparticles, and electrostatic

attraction facilitate the disordered phase formation of nanoparticles rather than crystalline phase formation [28]. The phytochemicals also contain a variety of functional groups, including amine, carbonyl, and hydroxyl groups, which can react with metal ions and reduce them into nanoparticles in a single process. The reaction with Zn^{2+} ions may entail the oxidation of OH groups, as the oxygen or hydroxyl compounds in the plant extract prefer to contribute an electron to the electrophile Zn complexes [29]. It may also involve a donor-acceptor mechanism that reduces electron-deficient zinc ions to create zinc atoms. According to the EDS data, two powerful peaks at 101 and 108 keV, corresponding to the optical absorption of the produced nanoparticle, and two weak peaks at 8.5 and 9.4 keV (Figure 1d), showed the peaks characterized by BZO-NPs, which are due to the surface plasmon resonance of BZO-NPs. According to the elemental analysis of the nanoparticle, the atomic percentage of zinc and oxygen is 36.57 and 38.79%, respectively, and the peaks at 1.01 and 0.75 keV, respectively, confirmed the purity of BZO-NPs.

Effect of BZO-NPs on Micro-Morphological and Biochemical Parameters

Plant growth generally refers to the biomass accumulated as a result of the balance between photosynthesis and respiration [30]. Substance accumulation, also defined as RGR, can be defined by the total chlorophyll content and RWC ratio. In our study, BZO-NP concentrations caused some changes in growth parameters ($P \leq 0.05$). RGR was lowest in control (8%), but it was highest at 50 and 100 mg L⁻¹ BZO-NP concentrations (10%), suggesting that NP treatment promoted basil growth (Figure 2). Since zinc serves as the structural and catalytic component of proteins and enzymes and as a co-factor for pigment biosynthesis [31], increasing BZO-NP in the medium increased the total amount of chlorophyll. The increase in the amount of chlorophyll supports biomass accumulation by positively affecting the photosynthetic mechanism. However, although RGR showed the highest value at 50 and 100 mg L⁻¹ (10%), total chlorophyll contents did not increase at the same rate. The total chlorophyll amount was determined as 7.62% and 5.91% at 50 and 100 mg L⁻¹, respectively. Zinc oxide NPs support chlorophyll biosynthesis up to a certain concentration, but completely suppress chlorophyll biosynthesis at concentrations of 200 mg L⁻¹ and above [32]. The fact that RGR is similar in both concentrations but the chlorophyll content is different may indicate that RWC may be the parameter that triggers growth. Because, RWC showed the highest value at both concentrations (87% and 86%). This showed that BZO-NP positively affected all growth parameters at 50 mg L⁻¹, but

negatively affected the chlorophyll content at higher concentrations. However, although the total amount of chlorophyll decreased to 100 mg L^{-1} , the high RWC ensured the continuity of growth. However, the decrease in RGR at BZO-NP 200 mg L^{-1} was paralleled by the decrease in RWC and total chlorophyll quantity. BZO-NP positively affects growth by increasing the water absorption potential of plants [33]. It is also seen in Figure 2 that BZO-NP applications positively affect basil growth up to a certain concentration.

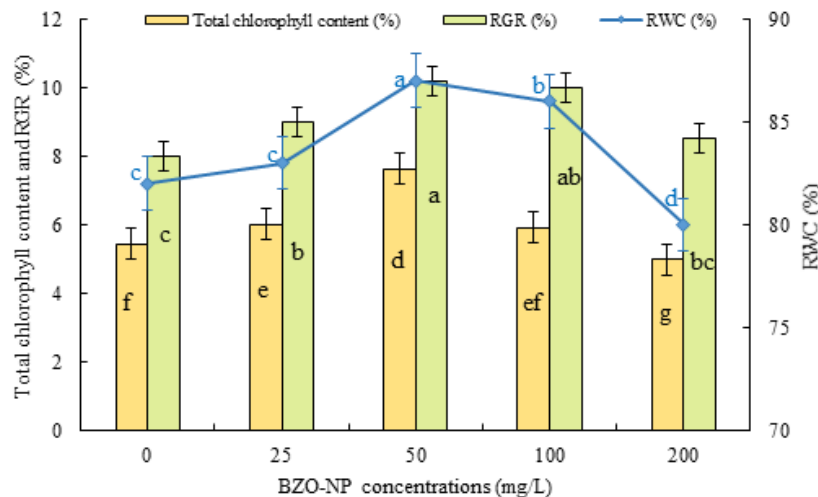


Figure 2. Effect of BZO-NP applications on basil growth on differences in RGR, RWC and total chlorophyll contents. Means \pm standard error are shown by vertical bars, and Tukey's test statistical differences are indicated by different letters ($P \leq 0.05$)

Since stomatal qualitative and quantitative changes in leaves directly affect the photosynthesis and respiration mechanism, plant growth can also be described by changes in stomatal movements. The responses of stomata to environmental variables are short-term, with changes in the opening-closing mechanism of the stomata, and long-term, with morphological changes occurring with the size, frequency and distribution of stomata [34]. These microscopic pores play a key role in improving crop yield as they regulate the photosynthesis and water use mechanism. BZO-NP treatments significantly affected stomata dimensions (length and weight), stomatal density and epidermis number ($P \leq 0.05$). Stomatal density reached its maximum value at 50 mg L^{-1} . In other concentrations, it showed lower values than stomatal density control (Figure 3a). While the epidermis number showed higher values than control at 25 and 50 mg L^{-1} , it was significantly lower than control at other concentrations (Figure 3b). Stomatal sizes decreased significantly with increasing concentration compared to control (Figure 3c-d). Changes in concentration revealed an inverse relationship between stomatal density and stomatal sizes. As a result of the increase in stomatal density with an increase in

concentration, the stomatal size decreased. Reducing the size of stomata organizes the continuity of photosynthesis by ensuring that the stomata pores remain open [35]. The inverse relationship between SPI and stomata size, especially the highest value at 100 mg L⁻¹, shows that our results support each other (Figure 3e). The decrease in stomatal density and the increase in the SPI, especially at 100 mg L⁻¹, can be defined as an effort to reduce the negative effect of decreasing stomatal density. Plants exposed to high temperatures enable adaptation to the environment by increasing stomata aperture despite low stomata densities [36].

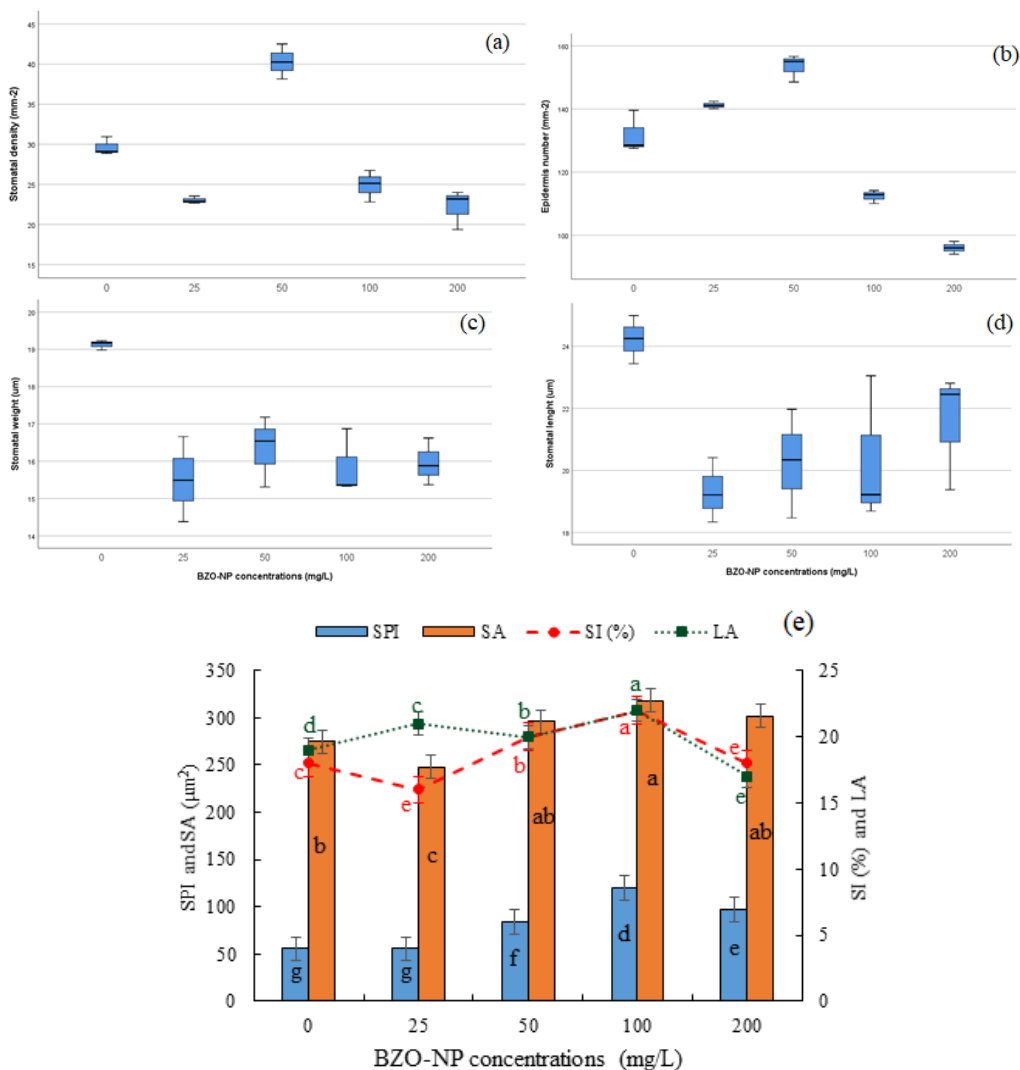


Figure 3. Changes in stomatal movements in response to BZO-NP applications in basil leaves. For graphs (Figure 3a-d), horizontal lines within boxes indicate the median and boxes indicate the upper (75%) and lower (25%) quartiles. The minimum and maximum value ranges are indicated with vertical bars, and significant differences between means are indicated with different letters.

To determine the effect of BZO-NP applications on the phenolic content of basil seedlings, the effect levels were determined by comparing 4 different concentrations of

BZO-NP with each other and with the control. Changes in peltate trichomes identified three different phenolic compounds (caffeic acid, rosmarinic acid and chlorogenic acid). Caffeic acid content decreased at BZO-NP 50 and 100 mg L⁻¹ compared to the control, but this decrease was not found to be statistically significant and the highest caffeic acid content was found at BZO-NP 200 mg L⁻¹. While rosmarinic acid content did not alter statistically at BZO-NP 100 mg L⁻¹, it increased significantly in other concentration treatments and the highest increase was observed in the BZO-NP 200 mg L⁻¹ treatment. Chlorogenic acid content increased with the rising treatment concentration, but between BZO-NP 25 and 50 mg L⁻¹, chlorogenic acid content did not change significantly and reached the highest value at BZO-NP 200 mg L⁻¹. Phenolic substance content increased in parallel with peltate trichomes (Figure 4).

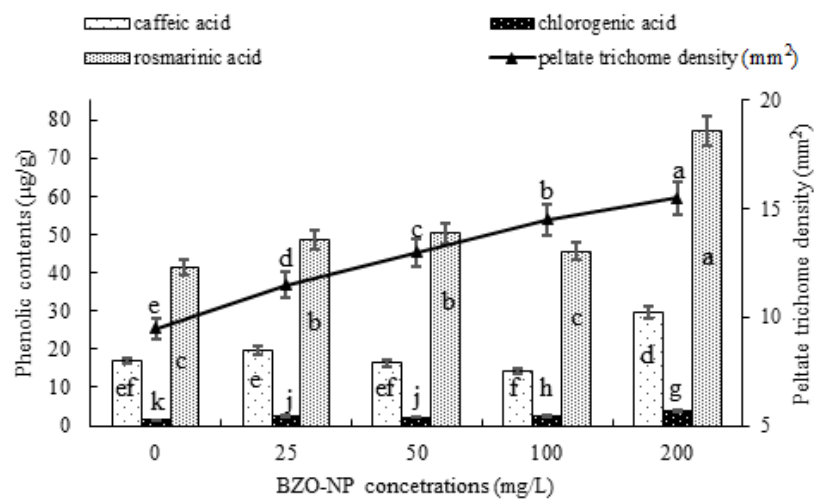


Figure 4. Phenolic content of basil seedlings in BZO-NP concentrations. Means \pm standard error are shown by vertical bars, and Tukey's test statistical differences are indicated by different letters ($P \leq 0.05$)

Glandular trichomes, which are responsible for producing, secreting and storing phytochemicals, are defined as metabolic cell factories [37]. The increase in glandular peltate trichomes, which are the production centers of phenolic acids, with BZO-NP treatments makes it possible to target the increase in the amount of phytochemicals. On the other hand, many reports describe that changes in phenolic substance content are associated with stomatal pore index results. The current study determined the inverse relationship between the increase in BZO-NP concentration and stomatal pore index and phenolic substance content. While the SPI was highest at BZO-NP 100 mg L⁻¹, it decreased at BZO-NP 200 mg L⁻¹ (Figure 3e). Similar changes were also seen in the amount of phenolic acid, and especially the amount of phenolic acids reached the highest value at BZO-NP 200 mg L⁻¹, and growth decreased (Figure 5). Phenolic compounds in

guard cells are effective in opening and closing the stomata [38]. Phenolic compounds accumulated in poplar plants reduced stomata opening, resulting in a decrease in CO₂ absorption and a photosynthetic decrease [39]. Changes in the amount of ABA, which causes stomatal closure due to inhibition of K⁺ uptake and increased ion flow from guard cells, are affected by the amount of phenolic acid [40].

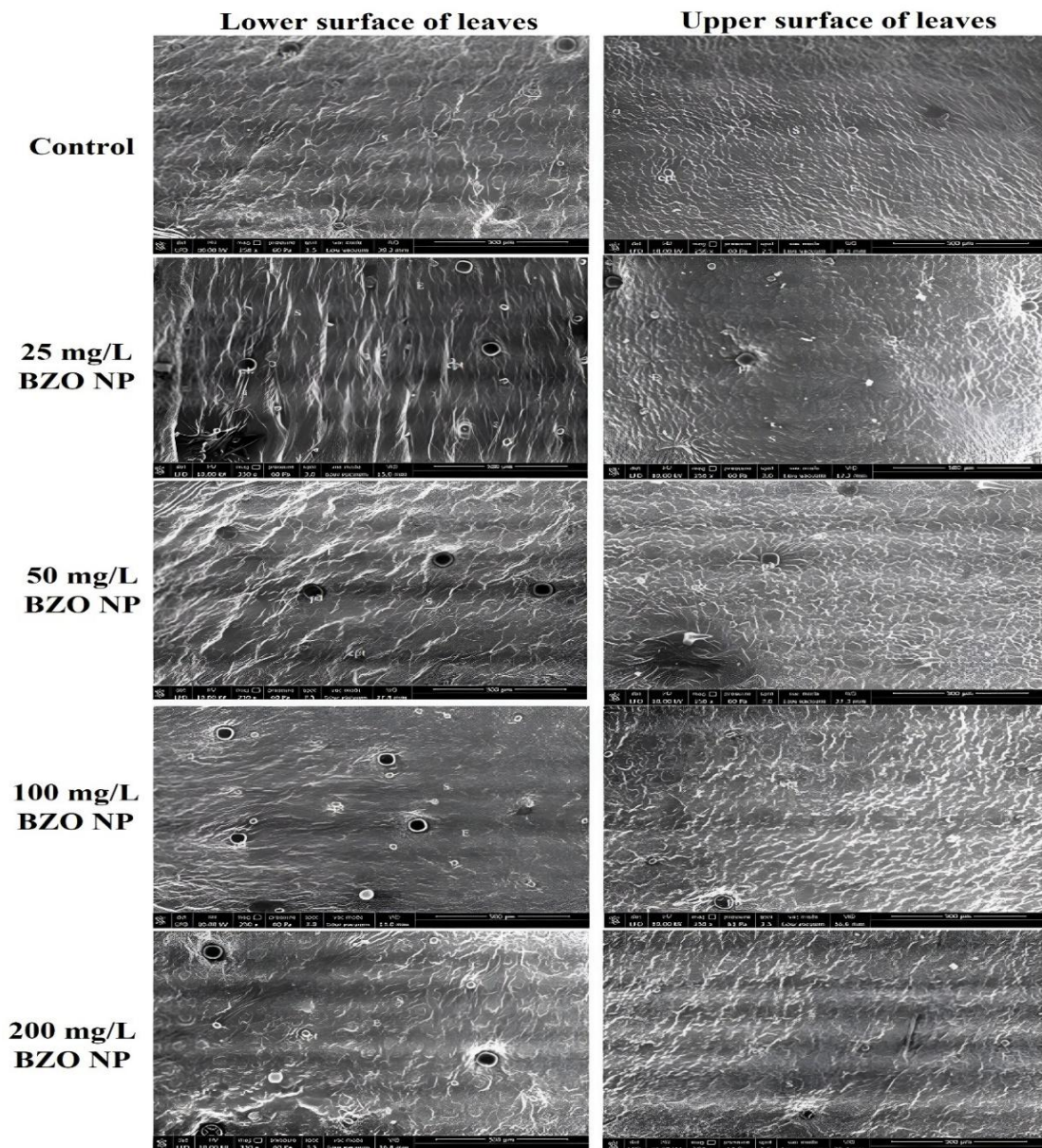


Figure 5. Responses of the structures of the epidermal system on the upper and lower surfaces of basil leaves to BZO-NP applications (S: stomata; E Epidermis; cpt: capitate trichome; plt: peltate trichome)

The treatment of different concentrations of BZO-NP to basil seedlings resulted in the identification of 81 essential oil components. Fifty-six of these compounds exhibited varying rates of increase or decrease compared to the control group. These compounds showed two different variations: compounds that were in control but decreased or were

not present in the treatments, and compounds that were not in control but were present and increased in the treatments. In this context, while methyl benzoate was found at $0.18 \mu\text{g g}^{-1}$ in the control group, it was not detected in any of the BZO-NP treatments. Linalyl acetate was found at $0.45 \mu\text{g g}^{-1}$ in the control, decreased by 45% at 25 and 50 mg L^{-1} in BZO-NP, 14% at 100 mg L^{-1} in BZO-NP and 20% at 200 mg L^{-1} in BZO-NP. Lavandulyl acetate was detected at $0.07 \mu\text{g g}^{-1}$ in the control, while it decreased by 72% at BZO-NP 25 mg L^{-1} and was not detected at all in other BZO-NP treatments. While methyl cinnamate was found to be $54.78 \mu\text{g g}^{-1}$ in the control, it decreased by 40%, 62%, 76% and 43% in BZO-NP 25, 50, 100 and 200 mg L^{-1} treatments, respectively. While geranyl isovalerate contained $0.59 \mu\text{g g}^{-1}$, nerolidol $0.45 \mu\text{g g}^{-1}$, hex-3(Z)-en-1-ol benzoate $0.07 \mu\text{g g}^{-1}$ and δ -cadinol $0.37 \mu\text{g g}^{-1}$ in the control, these compounds decreased in BZO-NP treatments and BZO-NP 200 mg L^{-1} could not be detected. Muurolol was found to be $2.07 \mu\text{g g}^{-1}$ in the control, while it decreased by 38%, 51%, 11% and 37% in BZO-NP 25, 50, 100 and 200 mg L^{-1} treatments, respectively. On the other hand, γ -Terpinene was not found in control and BZO-NP 200 mg L^{-1} , while it was found as $0.04 \mu\text{g g}^{-1}$, $0.06 \mu\text{g g}^{-1}$ and $0.05 \mu\text{g g}^{-1}$ in BZO-NP 25, 50 and 100 mg L^{-1} , respectively. While α -terpinolene and α -cedrene compounds could not be detected in the control, these components started to be synthesized as the treatment BZO-NP concentration increased and BZO-NP reached the highest value at 200 mg L^{-1} and was found to be $0.09 \mu\text{g g}^{-1}$ and $0.31 \mu\text{g g}^{-1}$, respectively. β -Myrcene was the compound that showed the highest increase, with an 83% increase at 50 mg L^{-1} , while it was $1.02 \mu\text{g g}^{-1}$ in the control. Compounds such as γ -terpinene, α -terpinolene and α -cedrene are inflammatory, that is, they are real antioxidants that prevent degradation by rapidly undergoing autoxidation [41, 42]. These compounds, which cannot be detected in the control group and whose amount increases with BZO-NP concentrations, are important compounds used in the treatment of various diseases. Capitata and peltate glandular trichomes in basil leaves are essential oil production and release centers [43]. The positive relationship between glandular hair density and essential oil yield [44] was also determined in BZO-NP treatments. The number of capitata glandular trichomes was 17, 22, 19, 21 and 18 in the control, 25, 50, 100, 200 mg L^{-1} BZO-NP treatments, respectively, while the number of peltate glandular trichomes was 9, 11, 13, 15 and 16, respectively. The contribution of BZO-NP applications to basil growth also affected the development of glandular trichomes. Growth is directly proportional to the highest increase in the number of glandular trichomes, especially at 100 mg L^{-1} . Variations in glandular trichome density were used to identify changes in the quantity and composition of essential oils. Similar findings have

been reported that the differences in the amount and composition of essential oils of 3 different *Satureja* plants are due to differences in glandular trichome density [45].

The activities of plant antioxidant enzymes such as SOD, CAT, GR, and APX, which are crucial for scavenging reactive oxygen species (ROS) that cause oxidative damage to lipids, proteins, and DNA [46], were affected by the foliar application of BZO-NPs. All concentrations of BZO-NP treatments led to a significant increase in SOD and CAT activity compared to the control (Figure 6a, b). SOD is responsible for defending cells against superoxide anion damage by converting it into H_2O_2 and O_2 . SOD activity in basil treated with 25 and 50 $mg L^{-1}$ BZO-NP increased by 120% and 153%, respectively, compared to the control. Two micronutrients that serve as SOD cofactors, Cu-Zn SOD and Fe-SOD, are responsible for the higher enzymatic activity of Cu-Zn SOD in the cytosol and Fe-SOD in the chloroplasts [47]. CAT activity was increased at 25, 50 and 100 $mg L^{-1}$ BZO-NP treatments compared to the control, but no significant difference was observed between concentrations. Treatment with ZnO NP significantly increased the uptake of Zn and Fe ions, which catalyze various biochemical reactions and enzyme cofactors [48]. Zinc also reduces ROS accumulation by increases the expression and activity of genes encoding antioxidant enzymes [49]. Exogenous treatment with ZnO NPs was also reported by Faizan and Hayat (2019) [50] to strengthen enzymatic defense mechanisms by increasing CAT and SOD activity.

GR is a key H_2O_2 scavenger in cells and plays a crucial role in the ascorbate-glutathione pathway. GR activity decreased by 30%, 17% and 28% in the 25, 50 and 100 $mg L^{-1}$ BZO-NP treatments compared to the control, with no significant differences observed among the concentrations (Figure 6c). It has been reported that plants exposed to heavy metals show a decrease in GR activity [51]. The decrease in GR activity under BZO-NPs could be associated with an increase in the oxidized glutathione pool [52].

APX activity increased by 13% and 18% in the 50 and 100 $mg L^{-1}$ BZO-NP treatments, respectively, while it decreased by 41% and 14% in the 25 and 100 $mg L^{-1}$ BZO-NP treatments comparison to the control (Figure 6d). Several studies have shown that exogenous treatment with ZnO-NPs improves APX activity [53, 54]. In the present study, differences were observed between the concentrations of BZO-NP treatments; however, 50 and 200 $mg L^{-1}$ BZO-NP were particularly effective in improving APX activity. The

results of enzymatic antioxidant activity suggest that the use of thyme extract in ZnO-NP synthesis could enhance the potential to reduce reactive oxygen species.

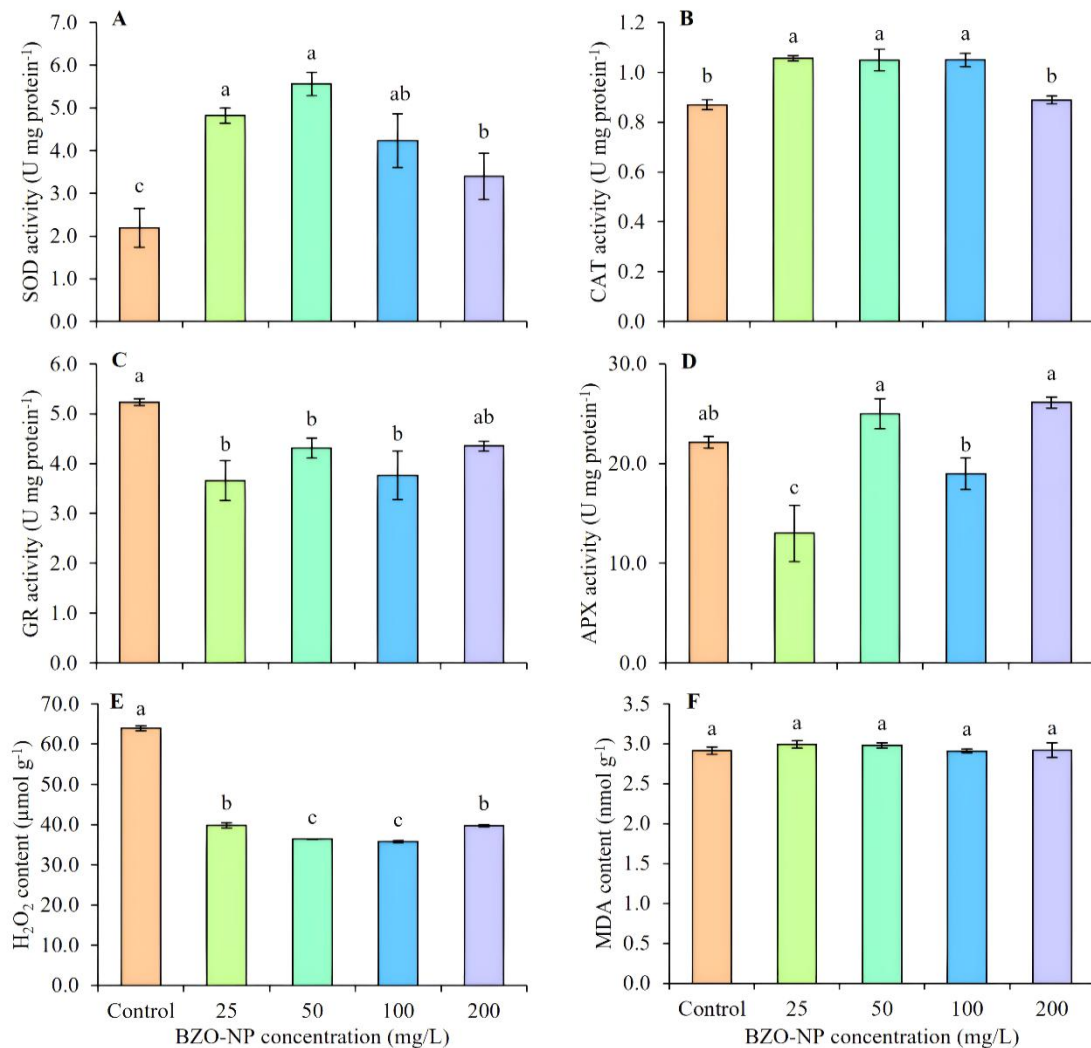


Figure 6. Effects of BZO-NP at different concentrations (0, 10, 50, 100, or 200 mg L⁻¹) on a) SOD, (b) CAT, (c) GR and (d) APX. The mean ± SE is represented by the data. Significant differences are indicated by different letters at P≤0.05.

All concentrations of BZO-NPs led to a significant reduction in H₂O₂ content compared to the controls. The 50 and 100 mg L⁻¹ BZO-NP treatments were the most effective in reducing H₂O₂ content, decreasing it by 42% and 43%, respectively, compared to the control. The results of the present study are supported by Sun et al. (2020) [55], who found that ZnO-NP treatment on maize leaves reduced H₂O₂ content. BZO-NP treatments significantly increased SOD and CAT activities in basil, which contributed to the reduction of H₂O₂ content. This, in turn, helps preserve the stability of chloroplasts and mitochondria. CAT is an important enzyme that catalyzes the conversion of H₂O₂ into H₂O and oxygen in peroxisomes [56] and it may have prevented H₂O₂ accumulation as a by-product through this role.

MDA is a by-product of lipid oxidation, which is triggered by ROS production [57]. Therefore, the amount of MDA reflects the extent of peroxidation and ROS production within the cell [52]. The results of this study revealed no significant differences in MDA content between the BZO-NP treatments and the control (Figure 6f). The MDA content in the 25, 50, 100, and 200 mg L⁻¹ BZO-NP treatments was 2.99, 2.98, 2.91, and 2.92 nmol g⁻¹, respectively. These results suggest that BZO-NPs enhance the activation of the enzymatic antioxidant system in basil, helping to eliminate the effects of ROS and prevent membrane peroxidation.

The result of Pearson linear correlation analysis based on the effect of different concentrations of BZO-NPs was provided in Figure 7. Out of the 66 correlation coefficients, 28 were negative and 38 were positive. While H₂O₂ content was negatively correlated with SOD activity ($r = 0.82$), it showed a positive correlation with GR activity ($r = 0.85$). SOD activity also showed a positive correlation with CAT activity ($r=0.89$). SPI is positively correlated with both SA ($r=0.92$) and PD ($r=0.86$) parameters. Additionally, Chl positively correlated with SD ($r=0.87$).

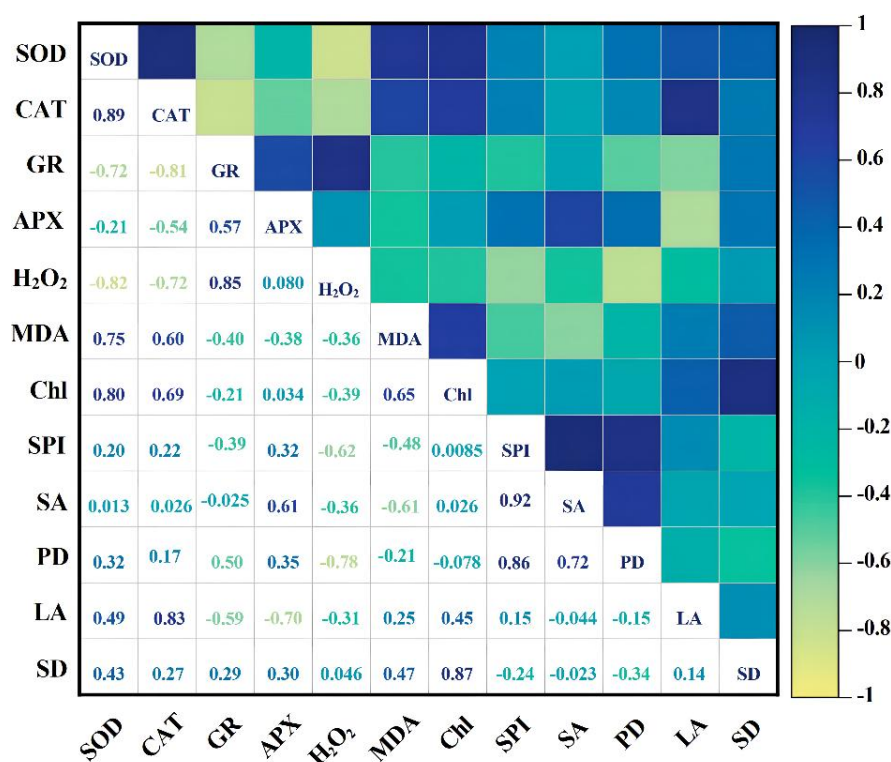


Figure 7. Heat map-generated relationships and correlations between biochemical and micro-morphological parameters utilizing mean values from basil following BZO-NPs treatment. The intensity of the normalized mean values of the different parameters is shown by the color scale (SOD, Superoxide dismutase; CAT, catalase; GR, glutathione reductase; APX, ascorbate peroxidase; H₂O₂, hydrogen peroxide; MDA,

malondialdehyde content; Chl, Chlorophyll content; SPI, Stomata Pore Index; SA, Stomatal area; PD, peltate trichome density; LA, Leaf area; SD, Stomatal density).

4. Conclusion

This study investigates the effects of different concentrations of BZO-NPs on the micro-morphological traits, essential oil composition, phenolic content, and biochemical parameters of basil plants. The treatment of BZO-NPs to basil seedlings in the pot experiment showed promising results. BZO-NP treatment positively influenced the growth of basil plants, as evidenced by changes in stomatal movements and increases in RGR, RWC, and total chlorophyll content. Changes in BZO-NP concentration revealed an inverse relationship between stomatal density and stomatal sizes: as the concentration of BZO-NPs increased, stomatal density increased, while stomatal size decreased. Similarly, a negative relationship was observed between the SPI and phenolic compound content with increasing BZO-NP concentration. The most effective micro-morphological parameters were observed at a BZO-NP concentration of 100 mg L⁻¹, where the number of glandular trichomes reached its maximum. Variations in the content and composition of essential oils were closely associated with changes in glandular trichomes density. Peltate glandular trichomes, responsible for phenolic production and release, were most abundant at 200 mg L⁻¹ BZO-NP, resulting in the highest production of rosmarinic acid at this concentration. Furthermore, BZO-NP treatments increased the activities of SOD and CAT, which are responsible for scavenging ROS, reduced H₂O₂ content and did not alter MDA content, thereby mitigating oxidative damage. These results underscore the agricultural potential of thyme extract-synthesized BZO-NPs, attributed to their eco-friendly and cost-effective properties.

Authorship contribution statement

S.Kilic and H.Kaya: Conceptualization; S. Kilic, S.Önder and D.Önder: Methodology; S. Kilic, S.Önder, D.Önder, H.Kaya: investigation, writing and editing.

Declaration of competing interest

The authors declare no competing interests.

Acknowledgment

Dr. Damla Önder passed away in August 2024 after contributing to the manuscript's conception, inspiration, and writing. She was a scholar at Molecular Biology Section of the Department of Biology at Süleyman Demirel University. Although she is no longer with us, we honor her memory and her contributions in this manuscript.

Ethics Committee Approval and/or Informed Consent Information

As the author of this study, I declare that I do not have any ethics committee approval and/or an informed consent statement.

References

- [1] C. Andreini, B. Ivano and R. Antonio, "Metalloproteomes: a bioinformatic approach", *Accounts of Chemical Research*, 42, 1471-1479. <https://doi.org/10.1021/ar900015x>, 2009.
- [2] J. Cherif, N. Derbel, M. Nakkach, H. Von Bergmann, F. Jemal and Z.B. Lakhdar, "Analysis of in vivo chlorophyll fluorescence spectra to monitor physiological state of tomato plants growing under zinc stress", *Journal of Photochemistry and Photobiology B: Biology*, 101, 332-339. <https://doi.org/10.1016/j.jphotobiol.2010.08.005>, 2010.
- [3] I. Tolay, "The impact of different zinc (zn) levels on growth and nutrient uptake of basil (*Ocimum basilicum* L.) grown under salinity stress" *PLoS One*, 16(2), e0246493, 2021.
- [4] Y. Orooji, M. Ghanbari, O. Amiri and M. Salavati-Niasari, "Facile fabrication of silver iodide/graphitic carbon nitride nanocomposites by notable photo catalytic performance through sunlight and antimicrobial activity", *Journal of Hazardous Materials*, 389, 122079. <https://doi.org/10.1016/j.jhazmat.2020.122079>, 2020.
- [5] M. Shahid, U. Naem-Ullah, W. Khan, D.S. Saeed and K. Razzaq, "Application of nanotechnology for insect pests management: A review", *Journal of Innovative Sciences*, 7, 28–39. <http://dx.doi.org/10.17582/journal.jis/2021/7.1.28.39>, 2021.
- [6] P. Sharma^a, M. Urfan, R. Anand, M. Sangral, H.R. Hakla, S. Sharma, R. Das, S. Pal and M. Bhagat, "Green synthesis of zinc oxide nanoparticles using *eucalyptus lanceolata* leaf litter: characterization, antimicrobial and agricultural efficacy in maize", *Physiology and Molecular Biology of Plants*, 28, 363-381. <https://doi.org/10.1007/s12298-022-01136-0>, 2022.
- [7] P. Pooja, A.S. Nandwal, M. Chand, A. Pal, A. Kumari, B. Rani, V. Goel and N. Kulshreshtha, "Soil moisture deficit induced changes in antioxidative defense mechanism of sugarcane (*Saccharum officinarum*) varieties differing in maturity" *Indian Journal of Agricultural Sciences*, 90(3), 507-512, 2020.
- [8] A. Salam, M.S. Afridi, M.A. Javed, A. Saleem, A. Hafeez, A.R. Khan, M. Zeeshan, B. Ali, W. Azhar, Z. Ulhassan and Y. Gan, "Nano-Priming Against Abiotic Stress: A way forward towards sustainable agriculture", *Sustainability*, 14:14880. <https://doi.org/10.3390/su142214880>, 2022.
- [9] V.D. Rajput, T.M. Minkina, A. Behal, S.N. Sushkova, S. Mandzhieva, R. Singh and H.S. Movsesyan, "Effects of zinc-oxide nanoparticles on soil, plants, animals and soil organisms: A review", *Environmental Nanotechnology, Monitoring & Management*, 9, 76-84. <https://doi.org/10.1016/j.enmm.2017.12.006>, 2018.
- [10] M. Faizan, F. Yu, C. Chen, A. Faraz and S. Hayat, "Zinc oxide nanoparticles help to enhance plant growth and alleviate abiotic stress: A review", *Current Protein & Peptide Science*, 22, 362-375. <https://doi.org/10.2174/1389203721666201016144848>, 2021.
- [11] R. Hunt, "Plant Growth Curves. The functional approach to plant growth analysis", Edward Arnold Ltd. London, UK, **ISBN: 9780713128444**, pp 248, 1982.
- [12] S.K. Pandey and H. Singh, "A simple, cost-effective method for leaf area estimation", *Journal of Botany*, 658240, 1-6. <https://doi.org/10.1155/2011/658240>, 2011.
- [13] B. Salisbury and W. Ross, "Plant Physiology", 4 th ed. Wadsworth, Belmont, California, pp. 682, 1992.
- [14] E. Rengifo, R. Urich and A. Herrera, "Water relations and leaf anatomy of the tropical species, *Jatropha gossypifolia* and *Alternanthera crucis*, grown under elevated CO₂ concentration", *Photosynthetica* 40:397-403. <https://doi.org/10.1023/A:1022679109425>, 2002.
- [15] N. Orcen, G. Nazarian and M. Gharibkhani, "The responses of stomatal parameters and SPAD value in asian tobacco exposed to chromium", *Polish Journal of Environmental Studies*, 22, 1441-1447, 2013.
- [16] L. Sack, P.D. Cowan, N. Jaikumar and N.M. Holbrook, "The 'hydrology' of leaves: Co-ordination of structure and function in temperate woody species", *Plant, Cell & Environment*, 26, 1343-1356. <https://doi.org/10.1046/j.0016-8025.2003.01058.x>, 2003.
- [17] G.W. Turner, J. Gershenzon and R.B. Croteau, "Development of peltate glandular trichomes of peppermint", *Plant Physiology*, 124, 665-680. <https://doi.org/10.1104/pp.124.2.665>, 2000.
- [18] V. Velikova, I. Yordanov and A.J.P.S. Edreva, "Oxidative stress and some antioxidant systems in acid rain-treated bean plants: protective role of exogenous polyamines", *Plant Science*, 151, 59-66. [https://doi.org/10.1016/S0168-9452\(99\)00197-1](https://doi.org/10.1016/S0168-9452(99)00197-1), 2000.
- [19] R.L. Heath and L. Packer, "Photoperoxidation in isolated chloroplasts: I. kinetics and stoichiometry of fatty acid peroxidation", *Archives of Biochemistry and Biophysics*, 125, 189-198. [https://doi.org/10.1016/0003-9861\(68\)90654-1](https://doi.org/10.1016/0003-9861(68)90654-1), 1968.

- [20] C.N. Giannopolitis and S.K. Ries, "Superoxide dismutases: I. occurrence in higher plants", *Plant Physiology*, 59, 309-314. <https://doi.org/10.1104/pp.59.2.309>, 1977.
- [21] B. Chance and A.C. Maehly, "Assay of catalases and peroxidases", [https://doi.org/10.1016/S0076-6879\(55\)02300-8](https://doi.org/10.1016/S0076-6879(55)02300-8), 1955.
- [22] Y. Nakano and K. Asada, "Hydrogen Peroxide is scavenged by ascorbate-specific peroxidase in spinach chloroplasts", *Plant Cell Physiology*, 22, 867-880. <https://doi.org/10.1093/oxfordjournals.pcp.a076232>, 1981.
- [23] M.M. Bradford, "A Rapid and sensitive method for the quantitation of microgram quantities of protein utilizing the principle of protein-dye binding", *Analytical Biochemistry*, 72, 248-254. [https://doi.org/10.1016/0003-2697\(76\)90527-3](https://doi.org/10.1016/0003-2697(76)90527-3), 1976.
- [24] K. Dulta, G. Koşarsoy Ağçeli, P. Chauhan, R. Jasrotia and P.K. Chauhan, "Ecofriendly synthesis of zinc oxide nanoparticles by *Carica papaya* leaf extract and their applications", *Journal of Cluster Science*, 33, 603-617. <https://doi.org/10.1007/s10876-020-01962-w>, 2022.
- [25] T. Khalafi, F. Buazar and K. Ghanemi, "Phycosynthesis and enhanced photocatalytic activity of zinc oxide nanoparticles toward organosulfur pollutants", *Scientific Reports*, 9, 6866. <https://doi.org/10.1038/s41598-019-43368-3>, 2019.
- [26] M.M. Chikkanna, S.E. Neelagund and K.K. Rajashekarappa, "Green synthesis of zinc oxide nanoparticles (ZnO NPs) and their biological activity", *SN Applied Sciences*, 1, 1-10. <https://doi.org/10.1007/s42452-018-0095-7>, 2019.
- [27] S. Modi, V.K. Yadav, N. Choudhary, A.M. Alswieleh, A.K. Sharma, A.K. Bhardwaj, S.H. Khan, K.K. Yadav, J.K. Vhron and B.H. Jeon, "Onion peel waste mediated-green synthesis of zinc oxide nanoparticles and their phytotoxicity on mung bean and wheat plant growth", *Materials* 15, 2393. <https://doi.org/10.3390/ma15072393>, 2022.
- [28] S. Thakur, M. Shandilya and G. Guleria, "Appraisalment of antimicrobial zinc oxide nanoparticles through *Cannabis*, *Jatropha curcusa*, *Alovera* and *Tinospora cordifolia* leaves by green synthesis process", *Journal of Environmental Chemical Engineering*, 9, 104882. <https://doi.org/10.1016/j.jece.2020.104882>, 2020.
- [29] S. Sharma^b, S.S. Singh, A. Bahuguna, B. Yadav, A. Barthwal, R. Nandan, R. Khatana, A. Pandey, R. Thakur and H. Singh, "Nanotechnology: An efficient tool in plant nutrition management. In Ecosystem Services: Types", Management and Benefits. Nova Science Publishers, Inc.: Hauppauge, NY, USA, 2022.
- [30] H. Lambers, R.S. Oliveira, H. Lambers and R.S. Oliveira, "Photosynthesis, respiration, and long-distance transport: photosynthesis", *Plant Physiological. Ecology*, 11, 114. https://doi.org/10.1007/978-3-030-29639-1_2, 2019.
- [31] V.L.R. Pullagurala, I.O. Adisa, S. Rawat, S. Kalagara, J.A. Hernandez-Viezas, J.R. Peralta-Videa and J.L. Gardea-Torresdey, "ZnO nanoparticles increase photosynthetic pigments and decrease lipid peroxidation in soil grown cilantro (*Coriandrum sativum*)", *Plant Physiology and Biochemistry*, 132, 120-127. <https://doi.org/10.1016/j.plaphy.2018.08.037>, 2018.
- [32] X. Wang, X. Yang, S. Chen, Q. Li, W. Wang, C. Hou and S. Wang, "Zinc oxide nanoparticles affect biomass accumulation and photosynthesis in arabidopsis", *Frontiers in Plant Science*, 6, 1243. <https://doi.org/10.3389/fpls.2015.01243>, 2016.
- [33] M.U. Hassan, M. Aamer, M. Umer Chattha, T. Haiying, B. Shahzad, L. Barbanti and H. Guoqin, "The critical role of zinc in plants facing the drought stress", *Agriculture*, 10, 396. <https://doi.org/10.3390/agriculture10090396>, 2020.
- [34] S.A. Casson and A.M. Hetherington, "Environmental regulation of stomatal development", *Current Opinion in Plant Biology*, 13, 90-95. <https://doi.org/10.1016/j.pbi.2009.08.005>, 2010.
- [35] T. Lawson, S. Von Caemmerer and I. Baroli, "Photosynthesis and stomatal behaviour", *Progress in Botany*, 72:265-304. https://doi.org/10.1007/978-3-642-13145-5_11, 2011.
- [36] R.S. Caine, X. Yin, J. Sloan, E.L. Harrison, U. Mohammed, T. Fulton and J.E. Gray, "Rice with reduced stomatal density conserves water and has improved drought tolerance under future climate conditions", *New Phytol.* 221, 371-384. <https://doi.org/10.1111/nph.15344>, 2019.
- [37] R. Schuurink and A. Tissier, "Glandular trichomes: micro-organs with model status?", *New Phytologist*, 225, 2251-2266. <https://doi.org/10.1111/nph.16283>, 2020.
- [38] A.M. Plumbe and C.M. Willmer, "Phytoalexins, water-stress and stomata: III. The effects of some phenolics, fatty acids and some other compounds on stomatal responses", *New Phytologist*, 103, 17-22. <https://doi.org/10.1111/j.1469-8137.1986.tb00592.x>, 1986.
- [39] K. Li, T. Zhang, H. Li, L.D. Zhang and F. Li, "Phenolic acids inhibit the photosynthetic productivity of poplar", *Photosynthetica*, 58:5. <https://doi.org/10.32615/ps.2020.071>, 2020.
- [40] R. Marchiosi, W.D. Dos Santos, R.P. Constantin, R.B. De Lima, AR. Soares, A. Finger-Teixeira and O. Ferrarese-Filho, "Biosynthesis and metabolic actions of simple phenolic acids in plants", *Phytochemistry Review*. 19, 865-906, 2020.

- [41] T.R. De Oliveira Ramalho, M.T.P. De Oliveira, A.L. De Araujo Lima, C.R. Bezerra-Santos and M.R. Piuvezam, "Gamma-terpinene modulates acute inflammatory response in mice", *Planta, Med.* 81, 1248-1254. <https://doi.org/10.1055/s-0035-1546169>, 2015.
- [42] J. Rudbäck, M.A. Bergström, A. Börje, U. Nilsson and A.T. Karlberg, "α-terpinene, an antioxidant in tea tree oil, autoxidizes rapidly to skin allergens on air exposure", *Chemical Research in Toxicology*, 25, 713-721. <https://doi.org/10.1021/tx200486f>, 2012.
- [43] C. Giuliani, M. Bottoni, L. Santagostini, A. Spada, A. Papini, F. Milani and G. Fico, "Teucrium fruticans L., a Multi-Scale Study: From Trichomes to Essential Oil", *Chemistry & Biodiversity*, 20:e202200913. <https://doi.org/10.1002/cbdv.202200913>, 2023.
- [44] E. Werker, E. Putievsky and U. Ravid, "The Essential oils and glandular hairs in different chemotypes of *Origanum vulgare* L.", *Annals of Botany*, 55, 793-801. <https://doi.org/10.1093/oxfordjournals.aob.a086958>, 1985.
- [45] T. Dodoš, S. Janković, P.D. Marin and N. Rajčević, "essential oil composition and micromorphological traits of *Satureja montana* L., *S. subspicata* Bartel ex Vis., and *S. kitaibelii* Wierzb. ex Heuff. plant organs", *Plants*, 10:511. <https://doi.org/10.3390/plants10030511>, 2021.
- [46] V.G.Uarrota, R. Moresco, E.C. Schmidt, Z.L. Bouzon, E. Da Costa Nunes, E. De Oliveira Neuber and M. Maraschin, "The Role of ascorbate peroxidase, guaiacol peroxidase, and polysaccharides in cassava (*manihot esculenta* crantz) roots under postharvest physiological deterioration", *Food Chemistry*, 197, 737-746. <https://doi.org/10.1016/j.foodchem.2015.11.025>, 2016.
- [47] S.N. Pandey, "In: Roychowdhury, R.; Choudhury, S.; Hasanuzzaman, M.; Srivastava, S. (Eds.). Role of Micronutrients in Biochemical Responses of Crops under Abiotic Stresses BT - Sustainable Agriculture in the Era of Climate Change", Springer International Publishing, Cham pp 93–112. https://doi:10.1007/978-3-030-45669-6_4, 2020.
- [48] W. Weisany, Y. Sohrabi, G. Heidari, A. Siosemardeh and H. Badakhshan, "Effects of zinc application on growth, absorption and distribution of mineral nutrients under salinity stress in soybean (*Glycine max* L.)", *Journal of Plant Nutrition*, 37, 2255–2269. <https://doi.org/10.1080/01904167.2014.920386>, 2014.
- [49] L.K. Mishra and A.B. Abidi, "Phosphorus-Zinc Interaction: Effects on yield components, biochemical composition and bread making qualities of wheat", *World Appl. Sci.* 10, 568–573, 2010.
- [50] M. Faizan and S. Hayat, "Effect of foliar spray of ZnO-NPs on the physiological parameters and antioxidant systems of *Lycopersicon esculentum*". *Polish Journal of Natural Sciences*, 34, 87-105, 2019.
- [51] A. Schützendübel and A. Polle, "Plant responses to abiotic stresses: heavy metal-induced oxidative stress and protection by mycorrhization", *Journal of Experimental Botany*, 53, 1351–1365. <https://doi.org/10.1093/jexbot/53.372.1351>, 2002.
- [52] D.K. Tripathi, R.K. Mishra, S. Singh, S. Singh, K. Vishwakarma, S. Sharma, V.P. Singh, P.K. Singh, S.M. Prasad, N.K. Dubey, A.C. Pandey, S. Sahi and D.K. Chauhan, "Nitric oxide ameliorates zinc oxide nanoparticles phytotoxicity in wheat seedlings: implication of the ascorbate-glutathione cycle", *Frontiers in Plant Science*, <https://doi.org/10.3389/fpls.2017.00001>, 2017.
- [53] H. Yasmin, J. Mazher, A. Azmat, A. Nosheen, R. Naz, M.N. Hassan and P. Ahmad, "Combined application of zinc oxide nanoparticles and biofertilizer to induce salt resistance in safflower by regulating ion homeostasis and antioxidant defence responses", *Ecotoxicology and Environmental Safety*, 218, 112262, 2021.
- [54] M.F. Seleiman, A. Ahmad, B.A. Alhammad and E. Tola, "Exogenous application of zinc oxide nanoparticles improved antioxidants, photosynthetic, and yield traits in salt-stressed maize", *Agronomy*, 13, 2645. <https://doi.org/10.3390/agronomy13102645>, 2023.
- [55] L. Sun, F. Song, J. Guo, X. Zhu, S. Liu, F. Liu and X. Li, "Nano-ZnO-induced drought tolerance is associated with melatonin synthesis and metabolism in maize", *International Journal of Molecular Sciences*, 21, 782. <https://doi.org/10.3390/ijms21030782>, 2020.
- [56] S.K. Panda, "Choudhury, S. Chromium Stress in Plants", *Brazilian Journal of Plant Physiology*, 17, 95-102, 2005.
- [57] M.M. Gaschler and B.R. Stockwell, "Lipid peroxidation in cell death", *Biochemical and Biophysical Research Communications*, 482, 419–42. <https://doi.org/10.1016/j.bbrc.2016.10.086>, 2017.